JOURNAL OF GEOPHYSICAL RESEARCH, VOL. 108, NO. C3, 8062, doi:10.1029/2000JC000715, 2003

# On the wave age dependence of wind stress over pure wind seas

William M. Drennan and Hans C. Graber
Rosenstiel School of Marine and Atmospheric Science, University of Miami, Miami, Florida, USA

Danièle Hauser and Céline Quentin
Centre d'étude des Environnements Terrestres et Planétaires (CETP), Vélizy, France

Received 13 November 2000; revised 11 June 2001; accepted 11 July 2001; published 13 March 2003.

[1] Data from five recent field campaigns are selected for pure wind sea, deep water, and fully rough flow conditions. The combined data set includes a wide range of wave ages, with high variability in both friction velocity and wave phase speed. These data, which are expected to follow Monin-Obukhov similarity scaling, are used to investigate the influence of wave age on wind stress. The relationship between the dimensionless roughness and inverse wave age is found to be $z_o/\sigma = 13.4\ (u_*/c_p)^{3.4}$, where $z_o$ is the surface roughness length, $\sigma$ is the standard deviation of the surface elevation, $u_*$ is the friction velocity, and $c_p$ is the wave phase speed at the peak of the spectrum. This relationship, which represents a significant dependence of roughness on wave age, was obtained using a procedure that minimizes the effects of spurious correlation in $u_*$. It is also shown to be consistent with the wave age relationship derived using an alternate form of the dimensionless roughness, namely, the Charnock parameter $z_o g/u_*^2$, where $g$ is the gravitational constant. *INDEX TERMS:* 4504 Oceanography: Physical: Air/sea interactions (0312); 4247 Oceanography: General: Marine meteorology; 4560 Oceanography: Physical: Surface waves and tides (1255); 3307 Meteorology and Atmospheric Dynamics: Boundary layer processes; *KEYWORDS:* wind stress, ocean waves, wind sea, wave age, roughness

**Citation:** Drennan, W. M., H. C. Graber, D. Hauser, and C. Quentin, On the wave age dependence of wind stress over pure wind seas, *J. Geophys. Res.*, *108*(C3), 8062, doi:10.1029/2000JC000715, 2003.

## 1. Introduction

[2] The air-sea fluxes of momentum, heat and mass in the marine atmospheric boundary layer (MABL) are key boundary parameters for atmospheric, oceanic and wave models. With the recent efforts to couple ocean and wave information to atmospheric models [e.g., *Hodur*, 1997; *Powers and Stoelinga*, 2000], accurate knowledge of the fluxes is increasingly important. As pointed out by *Powers and Stoelinga* [2000], "... marine roughness lengths [related to air sea fluxes] can be a linchpin in coupled air-sea mesoscale models, strongly influencing the strength of communication across the atmosphere/ocean interface". Similarly, the accurate modeling of near-surface processes in the ocean boundary layer depends strongly on the coupling [*Noh*, 1996].

[3] Direct measurement of these fluxes involves sampling the turbulent fluctuations of the relevant parameters (wind velocity, temperature, humidity) over a wide range of scales, and correlating them with concurrent and co-located measurements of the turbulent fluctuations of vertical velocity. For instance the momentum flux vector $\tau$ is given by

$$\tau = -\rho\left(\overline{u'w'}\,i + \overline{v'w'}\,j\right), \tag{1}$$

where $\rho$ is the air density, $u'$, $v'$ and $w'$ are the turbulent components of horizontal in-line (with the mean wind), horizontal cross-wind and vertical velocities, respectively, and the overbar refers to time averaging over a suitable period (typically of order 30 min). In the marine environment, such measurements are challenging, and are therefore sparse in both time and space. Consequently, fluxes are typically estimated using indirect methods such as the bulk method, which uses more readily measured mean quantities (wind speed, air and sea surface temperatures, etc.) together with empirical bulk transfer coefficients. For momentum transfer,

$$|\tau| = \rho C_z (U_z - U_o)^2, \tag{2}$$

where $C_z$ is the drag coefficient at $z$ meters above mean sea level, $U_z$ the mean $z$-meter wind speed and $U_o$ the surface drift speed, usually assumed to be zero.

[4] Given the importance of the bulk coefficients, much experimental and theoretical effort has been devoted to the development of accurate empirical relationships. That such relationships should exist follows from the similarity theory proposed by *Monin and Obukhov* [1954]. In a stationary and homogeneous atmospheric boundary layer, they postulated that there exists a layer near the surface where surface fluxes are constant. Then, assuming that the turbulence in


0148-0227/03/2000JC000715

the surface layer is generated by a combination of shear and buoyancy, they proposed that

$$\frac{(U_z - U_o)}{u_*} = \mathrm{f}\left(\frac{z}{z_o}, \frac{z}{L}\right), \tag{3}$$

where $u_* = (|\tau|/\rho)^{1/2}$ is the friction velocity, $z_o$ is the surface roughness length, and $L$, the Obukhov length, is given by

$$L = -u_*^3[\kappa g(H/(c_P T_o) + 0.61E/L_v)/\rho]^{-1}, \tag{4}$$

where $T_o$ is the reference potential temperature, $H$ the sensible heat flux, $E$ the latent heat flux, $c_P$ the specific heat at constant pressure, $L_v$ the latent heat of vaporization, $\kappa$ the von Kármán constant $\approx$0.4, and $g$ the gravitational acceleration. The roughness length $z_o$ is expected to be related to the physical roughness elements, the surface waves, only for flows which are aerodynamically rough. We use the roughness Reynolds number criterion $u_* z_o/\nu > 2.3$, where $\nu$ is the kinematic viscosity of air, to identify these cases. For reference, $\nu \approx 1.44 \times 10^{-5}$ m$^2$ s$^{-1}$ at 10°C.

[5] The Obukhov length is the height where turbulence production due to shear is balanced by turbulence production due to buoyancy. In neutral conditions, that is flow with negligible buoyant forcing, $L \rightarrow \infty$, and

$$\frac{(U_{zN} - U_o)}{u_*} = \frac{1}{\kappa} \log \frac{z}{z_o}, \tag{5}$$

where the subscript $N$ denotes neutral. This is the well known 'law of the wall' scaling. From (2) and (5), the neutral drag coefficient can be related to the roughness:

$$C_{zN} = \kappa^2[\log(z/z_o)]^{-2}. \tag{6}$$

Consequently, it is common to discuss the surface roughness length instead of $C_{zN}$.

[6] Based on dimensional reasoning, *Charnock* [1955] proposed $z_o = \alpha u_*^2/g$, where $\alpha$ is known as the Charnock parameter. Charnock took $\alpha$ as a constant, which implies $C_{zN} = \mathrm{f}(z, U_{zN})$. Although many bulk relations of this form have been proposed [see, e.g., *Geernaert*, 1990], there are significant differences between the various curves. A single relationship, one valid at all sites and in all conditions, remains elusive.

[7] *Kitaigorodskii and Volkov* [1965] suggested that $\alpha$ should be a function of a wave related parameter, such as the wave age, $c_p/u_*$, to account for the fact that the roughness elements are moving surface waves. Here $c_p$ is the phase speed of the surface waves at the spectral peak. Although experimental support for the proposed wave age dependence of $\alpha$ was first presented by *Donelan* [1982], it has remained controversial. Few other data sets have shown a strong wave age dependence. For a summary of recent results, see *Komen et al.* [1998].

[8] There are several reasons why it has been difficult to determine the validity of a wave age dependence. First of all, relationships (3)–(6) are only expected to be valid within the confines of Monin-Obukhov (MO) theory. Since the early work of *Volkov* [1970] and others, it has been recognized that in the presence of swell waves, classical MO-based turbulent scaling alone is inadequate. *Donelan et al.* [1993] concluded that the presence of significant swell precludes a relationship between roughness and wave age. This may, in part, be due to the behavior of the so-called wave boundary layer (WBL) during swell conditions.

[9] As discussed by *Phillips* [1977], the velocity field above surface waves can be separated into three components: a mean flow, the turbulent fluctuations, and a component coherent with the underlying wave field. Similarly, the stress can be partitioned into turbulent $\tau_t$, wave-coherent $\tau_w$, and viscous $\tau_v$ components, i.e., $\tau = \tau_t + \tau_w + \tau_v$. The viscous stress is significant only in a layer of O(1 mm) above the surface, and is neglected here. The wave-coherent stress $\tau_w$ accounts for the transfer of momentum to the waves. Away from the surface, $\tau_w \approx 0$ and the turbulent stress dominates the total stress. However near the surface, in the wave boundary layer, $\tau_w$ is significant. The turbulent stress is consequently reduced in the WBL (since the total stress, $\tau$, is constant) resulting in the neutral wind speed profiles deviating from their expected logarithmic forms [*Stewart*, 1961]. As a result, MO similarity theory does not apply in the WBL.

[10] Recent turbulence models [*Janssen*, 1989; *Makin and Mastenbroek*, 1996] predict the WBL height to be of O(1 m) for pure wind sea conditions, implying that MO theory is valid at typical measurement heights of O(10 m) over wind seas. This is supported by recent experimental evidence [*Edson and Fairall*, 1998; *Drennan et al.*, 1999]. Drennan et al. showed that turbulent velocity spectra and co-spectra for pure wind sea conditions follow the universal forms predicted by MO theory [see *Miyake et al.*, 1970]. These spectra, measured at heights ranging from 2 to 12 m above mean water level, represent a wide variety of wind speeds, with wave ages from very young to fully developed. Hence pure wind sea data are expected to follow MO theory, except within O(1 m) of the surface.

[11] On the other hand, in the presence of swell the WBL may extend well beyond typical measurement heights. Recent support for this was presented by *Drennan et al.* [1999] who showed that the universal spectral scaling of $u'$, $w'$ and $u'w'$ breaks down when 'strong swells' (swells much more energetic than the wind sea) are present. Also, *Donelan* [1990] and *Smedman et al.* [1999] showed that neutral wind speed profiles in the MABL are no longer logarithmic (as predicted by MO theory) when strong swells were observed. Hence, the validity of MO theory must be questioned when applied to measurements made over swell waves.

[12] These conclusions are based on data collected during light wind ($U_{10} < 5$ m s$^{-1}$), strong swell, conditions. More typical of the open ocean are so-called mixed-seas, when the swell and wind sea components are of roughly the same magnitude. It is not yet clear whether the strong-swell effects reported above, and also by *Donelan et al.* [1997] in similar conditions, persist in the mixed-sea regime. However, existing observations in mixed seas indicate that the presence of swell can modify, and increase the scatter in the drag coefficient relations compared to the pure wind sea regime [*Volkov*, 1970; *Geernaert et al.*, 1986; *Rieder*, 1997; *Donelan et al.*, 1997]. In the work that follows we exclude all swell data in order to maximize the likelihood that MO theory is valid.

[13] The presence of shoaling waves also affects the validity of MO theory. *Anctil and Donelan* [1996] and *Oost* [1998] have shown that shoaling waves can lead to a modified drag relation, with the surface roughness enhanced by wave breaking. Once again (3)–(6) are not expected to be valid in these conditions, as the atmospheric turbulence may depend on an additional parameter, one related to the water depth.

[14] Another problem plaguing studies seeking to validate the wave age dependence of roughness relates to the use of a single data set in the analysis [*Smith et al.*, 1992; *Johnson et al.*, 1998]. In particular, many data sets have relatively little variation in $c_p$ compared to $u_*$, and hence variability in wave age is almost entirely due to variability in friction velocity. In the well known HEXOS data set, $9.0 < c_p < 11.3$ m s$^{-1}$, while $0.33 < u_* < 1.11$ m s$^{-1}$ [*Janssen*, 1997]. Since $u_*$ is also commonly used to form a dimensionless roughness variable (see below), the result is that an apparent correlation between dimensionless roughness and wave age can be spurious, resulting from the dependence of both roughness and wave age on $u_*$ [*Kenney*, 1982].

[15] Here we study the influence of wave age on wind stress using field data that are carefully selected so as to follow MO theory. We restrict the data to pure wind sea, deep water and fully rough flow conditions. We use five recent data sets, each of which combines direct (eddy correlation) wind stress and directional wave data. The combined data set includes a wide range of wave ages, with high variability in both $u_*$ and $c_p$. Consequently, it is possible to greatly reduce the effect of spurious correlation on the wave age relationship.

## 2. FETCH Experiment

[16] The FETCH (Flux, État de la mer et Télédétection en Condition de fetch variable, or Flux, sea state, and remote sensing in conditions of variable fetch) experiment took place from 12 March to 16 April 1998 in the Gulf of Lion, Mediterranean Sea. An overview of the experiment is given by *Hauser et al.* [2003]. One of the goals of FETCH was to improve the parameterization of turbulent fluxes of momentum and heat with particular emphasis on fetch-limited situations and high wind conditions. During FETCH, fluxes were measured from three platforms. Momentum flux was measured by eddy correlation from a moored Air-Sea Interaction Spar (ASIS) buoy (Figure 1); momentum, heat and humidity fluxes were measured using the inertial dissipation method from the ship N.O. *L'Atalante*; eddy correlation fluxes were measured on a few occasions from an aircraft. Here we focus on the ASIS data, as only for these data are there coincident wave spectra. See *Dupuis et al.* [2003] for results from the *L'Atalante* data set.

[17] An ASIS buoy [*Graber et al.*, 2000] was deployed at 42° 58′ 56″N, 04° 15′ 11″E, roughly 50 km SSW of the Rhone delta at a depth of 100 m. The buoy is a multispar design, using five slender cylinders (0.22 m diameter by 3.5 m length) at the apices of a pentagonal cage of radius 1.1 m. The five spar elements are joined to a larger single spar column approximately 2.7 m below the mean surface level, and this central spar is terminated with a drag plate. The overall length of the buoy is 9 m. ASIS is designed specifically for research at the air-sea interface: it is both stable (with pitch and roll motions about one third those of a 3 m discus buoy) and aerodynamically clean. During FETCH, the ASIS buoy was deployed in a moored configuration, tethered to a secondary buoy so as to isolate additional downward forces.

**Figure 1.** Photograph of the ASIS (left) and tether buoys deployed during FETCH. For scale, the mast on ASIS has a height of 4 m.

### 2.1. Atmospheric Turbulence Measurements

[18] The mission of ASIS during FETCH was to provide measurements of turbulent momentum fluxes and directional wave spectra, along with supporting mean MABL and oceanic measurements. For fluxes, ASIS was equipped with a Gill 3-axis Solent sonic anemometer (model 1012R2A), yielding the full 3D wind vector, along with sonic temperature. The anemometer was mounted on top of a 4 m meteorological mast, with the sensing volume at the height of 7 m above the mean surface level. A motion package consisting of 3 orthogonal pairs of rate gyros (Systron Donner GC1-00050-100) and linear accelerometers (Columbia Research Laboratory SA-307HPTX), along with a compass (Precision Navigation TCM-2), was located in an underwater housing at the base of the buoy. These sensors yield all six components of motion of the buoy, and the signals are used to transform the wind velocity measurements to a stationary reference frame. Details of the motion correction algorithm are given by *Anctil et al.* [1994] and *Graber et al.* [2000]. A Rotronic temperature/relative humidity sensor (model MP-100C) mounted on the mast at 5 m provided mean measurements of air temperature and relative humidity. A temperature transducer mounted 2 m below mean surface level recorded water temperature.

[19] Data were sampled continuously at 12 Hz for 57 min, and stored on board. Data were subsequently processed in blocks of 28.5 minutes. The time series were screened for spikes. After application of the motion correction algorithm, the horizontal velocities were rotated into the mean wind direction. A mean tilt correction was applied to the wind velocities forcing $\overline{w} = 0$. The anemometer employs an asymmetric head design; those data where the mean wind direction was from the back of the sonic, through the probe supports, were rejected. The wind stress vector $\tau$ was calculated after first detrending the data. The data were

transformed to neutral values using the flux profile relations, $\psi_u$ ($z/L$), from *Donelan* [1990]:

$$U_{zN} = U_z + \left(u_*/\kappa\right)\psi_u(z/L). \quad (7)$$

During FETCH, the heat and moisture fluxes ($H$ and $E$) used to compute $L$ via (4) were not measured directly on ASIS, but calculated using bulk relations with constant Dalton and Stanton numbers of 0.0012 [*Smith*, 1989]. These values are very close to the recent ones of *DeCosmo et al.* [1996]. As these bulk relations require neutral values as input, an iterative algorithm is used. The iterative algorithm for $L$ was convergent in all wind sea cases.

### 2.2. Wave Measurements

[20] Directional wave measurements were made using 6 capacitance wave gauges mounted in a centered pentagonal array, with one gauge on each of the five faces of the buoy, and a sixth in the center. The wave gauge data were combined with the buoy motion data to obtain the true surface elevation [see *Drennan et al.*, 1994, 1998]. A standard array processing technique, the maximum likelihood method [*Capon*, 1969], was then applied to obtain directional wave spectra. As several of the FETCH goals depended on an accurate knowledge of the surface wave field, particularly its development as a function of fetch, wave measurements were also made by two waverider buoys, and a Merlin-IV aircraft carrying RESSAC radar [*Pettersson et al.*, 2003].

[21] To classify each spectrum as pure wind sea or not, we use an automatic selection scheme. This selection is based on the analysis of directional spectra as multiple wave systems. *Gerling* [1992] proposed the partitioning of wave spectra into wave trains. His original decomposition scheme was modified and adapted for wave prediction models [*Komen et al.*, 1994].

[22] The wave train decomposition consists of finding maximum values (peaks) of energy in the directional spectrum and isolating the associated wave trains. A wave train is limited by local minima around the peak, and with spreading less than 45° on both sides of the peak direction. The directional spectrum is partitioned into at most five wave trains. The main parameters such as mean period, mean propagation direction, and RMS surface elevation, are calculated for each wave train. If two wave trains are close in period and direction, they are combined together. The main parameters are then recalculated. Only four wave trains, those with the most energy $E$, are kept. Here, $E = \int\int S_{\eta\eta}(f, \theta)\, d\theta df$ where $S_{\eta\eta}$ is the two dimensional energy spectrum of surface elevation ($\eta$), $f$ is frequency and $\theta$ is propagation direction. An example of a bimodal wave system (wind sea plus swell) is given in Figure 2. The corresponding one dimensional frequency spectrum, $S_{\eta\eta}(f) = \int S_{\eta\eta}(f, \theta) d\theta$, is also shown. For future reference we introduce $\sigma$, the RMS surface elevation, and the significant wave height, $H_s = 4\sigma = 4E^{1/2}$.

[23] At most one wave train is identified as wind sea: the most energetic wave train which meets the criteria $U_{10N}\cos(\theta_d) > 0.83\, c_p$ [*Donelan et al.*, 1985] and $|\theta_d| < 45°$, where $\theta_d$ is the angle between the mean wind and peak wave train directions. The latter criterion ensures that the wave field identified as wind sea does, in fact, travel in the wind direction. Any other wave trains are classified as swells. Wind sea and swell energy are compared to determine if swells can be neglected. In order to reduce, to the greatest degree possible, the effects of swell on the roughness, we restrict the class of pure wind seas to those sea states where any swell energy is very small compared to that of the wind sea: E(swell) $\ll$ E(wind sea). In practice, we take this to be E(swell) < 5 E(wind sea). This is a conservative definition. We anticipate the results for 'pure wind seas' to be applicable to situations of light-moderate swells, albeit with the likelihood of additional scatter.

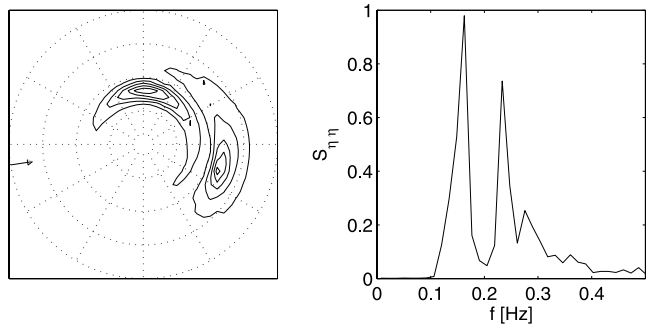


**Figure 2.** Sample ASIS directional wave spectrum from 6 April 1998, 06 Z. The left-hand plot shows the 2D spectrum, with north and east at the top and right, respectively. The wave trains are shown in the direction of propagation. The equispaced contours represent energy, and the four dotted circles represent frequencies 0.1, 0.2, 0.3, and 0.4 Hz. The right-hand plot shows the 1D wave spectrum. This is a case of complex sea. It is decomposed into two wave trains: wind sea, with $H_s$ = 0.59 m, $f_p$ = 0.26 Hz, $\theta_p$ = 107°, $c_p$ = 6.08 m s$^{-1}$; and one swell train, with $H_s$ = 0.60 m, $f_p$ = 0.16 Hz, $\theta_p$ = 11°, $c_p$ = 9.83 m s$^{-1}$. The wind, identified with the arrow on the left-hand plot, is 6.6 m s$^{-1}$, from −99°.

## 3. FETCH Data

[24] ASIS was deployed on 18 March (Julian day 77) 1998, and remained on site until recovery on 10 April (JD99). During that time ASIS operated continuously with the exception of a 12 hour period on JD91 when it was recovered for maintenance and data backup. On JD90, there were no anemometer data due to problems with the power supply. The FETCH data set includes 1070 runs of 28.5 min. Of these 831 were considered valid for stress data.

[25] The conditions during FETCH are summarized in Figure 3. The 10 m neutral wind speed is plotted in Figure 3a; the wind direction is given in Figure 3c. Of particular note are the Mistral events of JDs 79–80 and 83. The Mistral is a regional wind occurring during conditions of high pressure over western Europe/Bay of Biscay, combined with a low pressure system south of the Alps. The resulting winds are reinforced by orographic effects (Alps and Rhone valley). The Mistral, a northerly wind, is well known for its strong, steady and cold flow with near surface wind speeds sometimes in excess of 30 m s$^{-1}$. The latter half of the experiment was characterized by a sequence of four moderate fronts, with offshore (northerly) winds at the

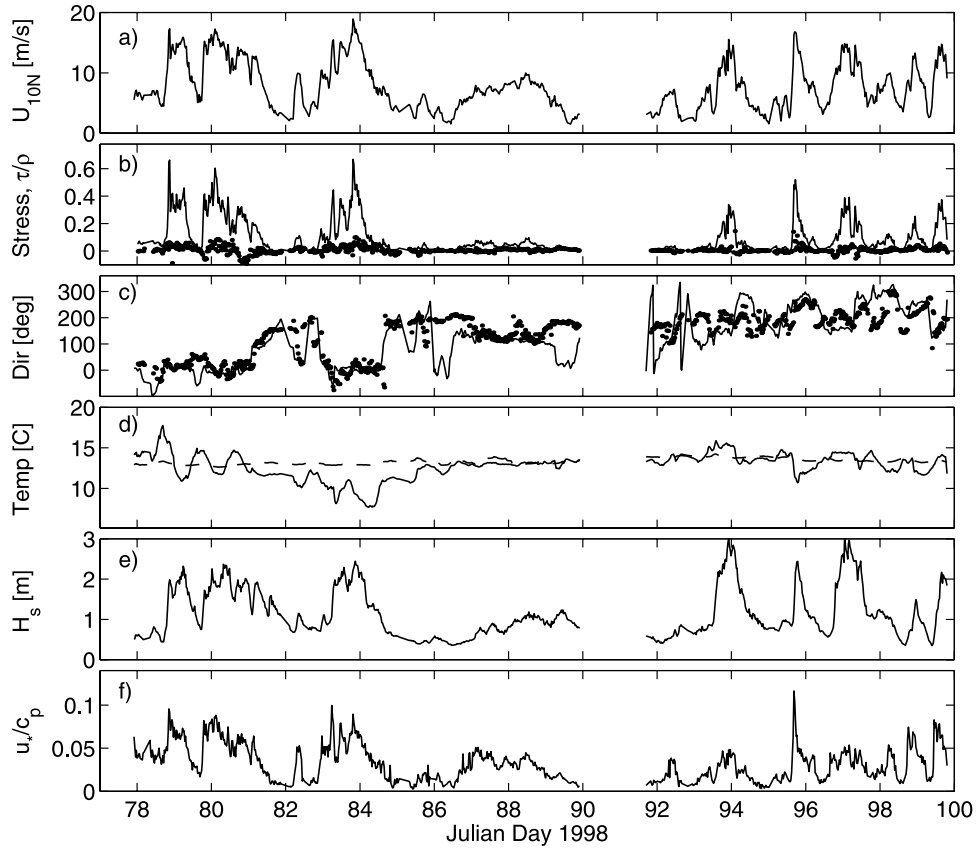


**Figure 3.** Meteorological and wave conditions during FETCH. The data shown are (a) 10 m neutral wind speed, (b) inline and cross-wind (dots) stress, $\tau/\rho$ [$m^2$ $s^{-2}$], (c) wind and peak wave (dots) directions, (d) air and sea (dashed line) temperatures, (e) significant wave height, and (f) inverse wave age.

rear of each event. The wind stress (in-line and cross wind components) is shown in Figure 3b, and the air and sea temperatures are shown in Figure 3d. The air-sea temperature difference is typically small (±2°C), except for the Mistral periods when cooler air is being advected in from the continent. The significant wave height is given in Figure 3e. Note that the highest waves occur not with the high wind Mistral events, which are fetch limited, but with the later frontal passages. Also shown are the wave direction at the spectral peak (Figure 3c) and the inverse wave age (Figure 3f).

[26] In Figure 4 the 10 m neutral drag coefficient is plotted versus $U_{10N}$ for the full FETCH data set. The data are well described in the mean by the *Smith* [1980] relation, except at the higher wind speeds where *Smith* [1980] underpredicts the data. It is evident from Figures 3a and 3f that these higher wind speed values are usually associated with younger waves (higher values of $u_*/c_p$), indicating possible support for a wave age effect. This is explored further below. At the lower wind speeds, the data exhibit considerable scatter, as is typical in such relations. *Mahrt et al.* [1996] discuss several flux sampling problems which are expected to lead to increased scatter in these conditions. Also, as pointed out above, the effect of swell on momentum flux has been particularly evident at low winds. To eliminate the swell effect, we now restrict ourselves to the subset of data consisting of pure wind sea events. These data are distinguished in Figure 4. As is typical in the ocean, there are few pure wind sea data for $U_{10N} < 6$ m $s^{-1}$; swells dominate in these conditions.

[27] It is common to use the Charnock parameter, $\alpha$, as the dimensionless roughness, and to seek a relation of the form $\alpha = z_o g/u_*^2 = f(c_p/u_*)$. This has the disadvantage that both the dimensionless roughness and the wave age depend strongly on the friction velocity. Consequently, a 'significant' correlation between $\alpha$ and $c_p/u_*$ may in fact be spurious, arising from the fact that both variables are themselves highly correlated to $u_*$. Here we prefer the scaling of roughness on wave height, as proposed by *Kitaigorodskii* [1970] and subsequently used by *Donelan* [1990]. We note that this scaling is not completely free of potential self-correlation, as the roughness is not measured directly, but calculated from $u_*$ via (5).

[28] In Figure 5 we plot the dimensionless roughness, $z_o/\sigma$ versus inverse wave age. The FETCH wind sea data are in qualitative agreement with the curve of *Donelan* [1990], showing increasing roughness for younger waves, although there is considerable scatter particularly for older waves (lower $u_*/c_p$). As the waves approach full development, it becomes more difficult to distinguish wind sea from swell. As discussed above, the addition of swell increases the variability of the stress (and hence roughness), as well as increasing the wave height over the pure wind sea value.

[29] For the FETCH data the range in peak phase speed is roughly a factor of 2.2, from 5 to 11 m $s^{-1}$, which compares with a factor of 3.9 variation in $u_*$ (see Figure 6 and Table 1).

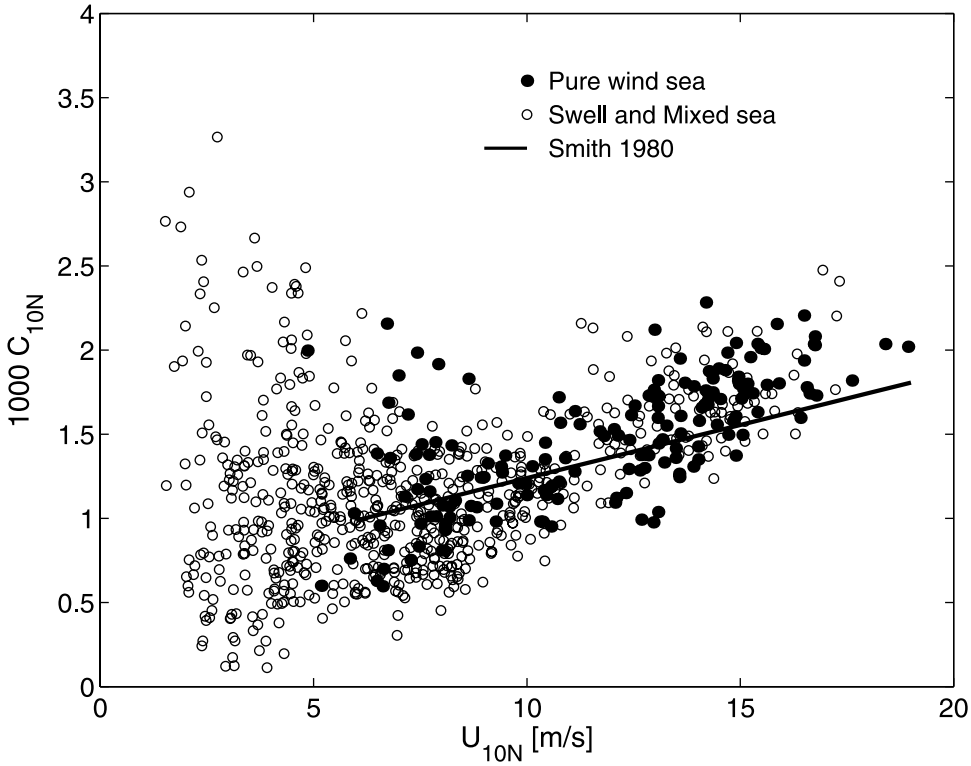


**Figure 4.** Drag coefficient versus wind speed, both 10 m neutral, for the FETCH experiment. Pure wind sea data are distinguished from the swell and mixed sea cases. Four low wind swell cases lie outside of the range of the plot axes.

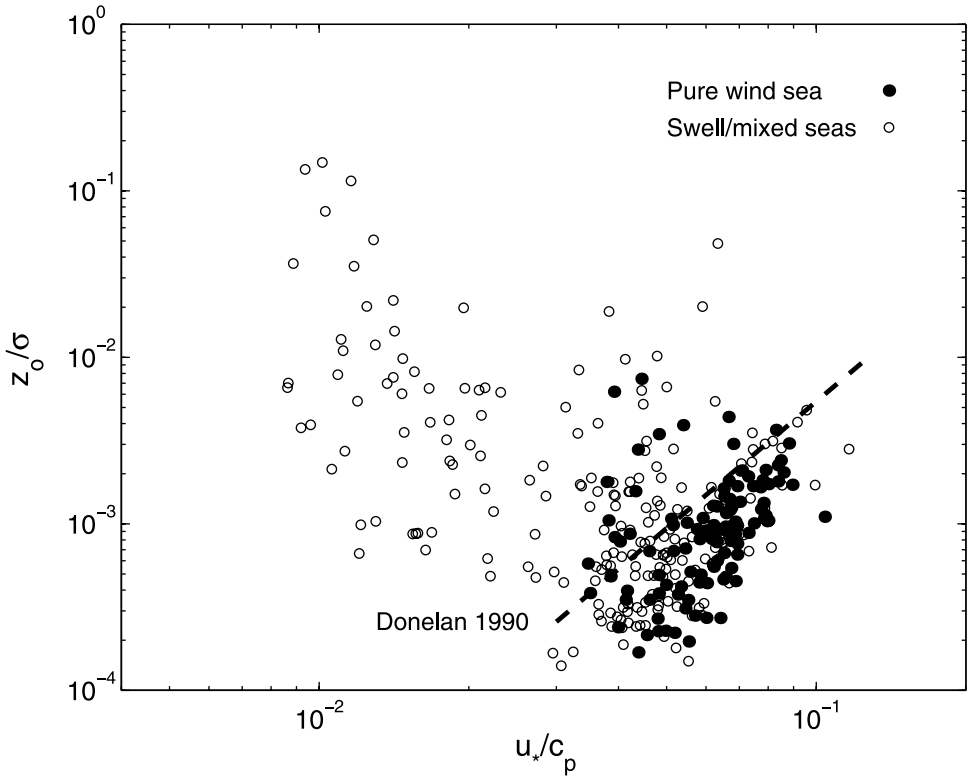


**Figure 5.** Dimensionless roughness versus inverse wave age for the FETCH data. The pure wind sea data meeting the rough flow criterion $z_o u_*/\nu > 2.3$ are identified with solid circles. Here $z_o$ is the roughness length, $\sigma$ is the standard deviation of the surface elevation, $u_*$ is the friction velocity, $c_p$ is the peak wave phase speed, and $\nu$ is the kinematic viscosity of air.

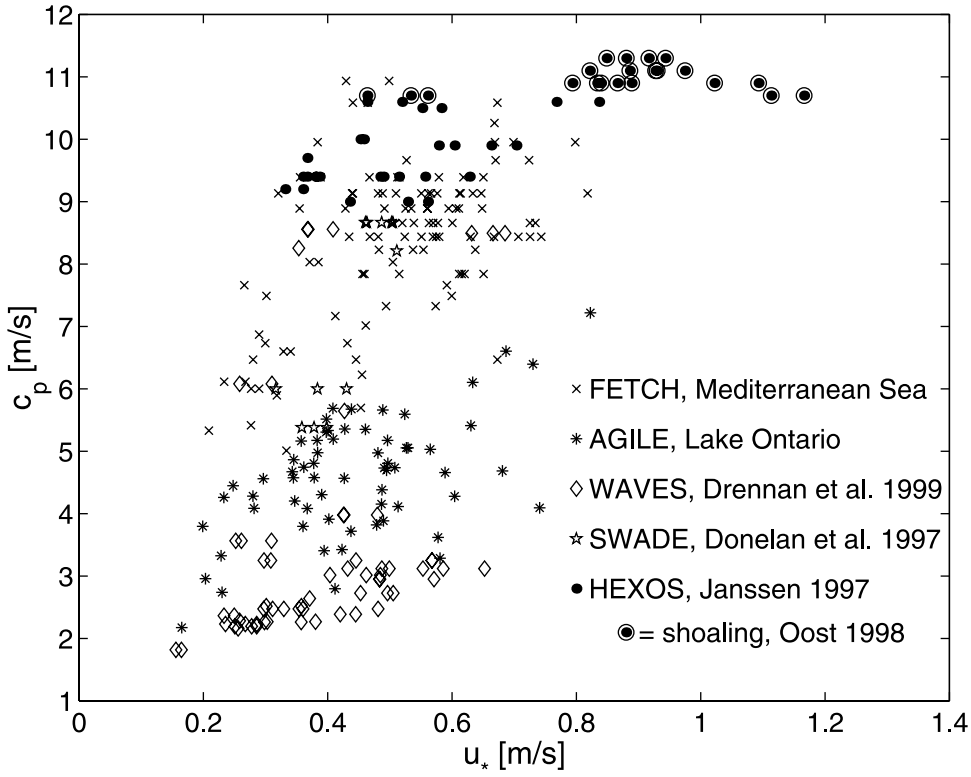


**Figure 6.** Distribution of friction velocity $u_*$ and peak phase speed $c_p$ for the five pure wind sea data sets considered here. The HEXOS data identified as shoaling by *Oost* [1998] are identified on the plot and omitted from the data set.

In contrast, the classical HEXOS data set has a factor 2.5 variation in $u_*$, but only 1.2 in $c_p$. Although the $c_p$ range is larger for the FETCH data than for the HEXOS data, $u_*$ remains the dominant source of variability in wave age. Hence spurious correlation remains a potential problem. We therefore choose to extend the analysis to include several other data sets representing different conditions. This approach, resulting in wider, and now roughly equal, ranges of $u_*$ and $c_p$, allows us to reduce, to the greatest possible degree, any effects of spurious correlation in the analysis. Below, we introduce four recent data sets combining eddy correlation stress and directional wave measurements. The data, collected at different sites and from different platforms, complement the FETCH data and considerably increase the range of phase speed and wave age. These data are summarized in Table 1.

[30] This approach of using multiple data sets to extend the parameter range was used by *Johnson et al.* [1998] who treated each data set as a single data point, and sought a relationship between the averaged dimensionless roughness and wave age. We follow a similar approach here, with two important differences: we include only data collected in pure wind sea, deep water, conditions, and we do not average the data sets. Although the approach of averaging data may be reasonable for experiments with narrow parameter ranges, it leads to very wide error bars for the data considered here. Instead, we consider all data as representative of pure wind sea conditions, and treat all data points equally.

## 4. Other Wind Sea Data

### 4.1. WAVES

[31] The WAVES (Water-Air Vertical Exchange Study) experiment was conducted from a tower at 12 m depth, 1.1 km from the western shore of Lake Ontario [*Donelan et al.*, 1999]. Wind stress measurements were made from a bivane at 12 m above mean water level, and directional wave spectra were calculated from an array of six capacitance wave gauges. Here we use data from the 1987 field season [*Drennan et al.*, 1999]. The subset of pure wind sea data was selected using the same criteria as above. Sixty-three 30 min runs met the criteria. The parameter range of these data

**Table 1.** Experimental Data

| Campaign | Reference | Points | $U_{10N}$, m s$^{-1}$ | $u_*$, m s$^{-1}$ | $c_p$, m s$^{-1}$ | $u_*/c_p$ |
|---|---|---|---|---|---|---|
| FETCH | this study | 110 | 4.9–18.9 | 0.21–0.82 | 5.0–10.9 | 0.03–0.10 |
| WAVES | *Drennan et al.* [1999] | 63 | 4.0–14.6 | 0.16–0.69 | 1.8–8.6 | 0.04–0.21 |
| AGILE | *Donelan and Drennan* [1995] | 64 | 4.0–14.9 | 0.17–0.82 | 2.2–7.2 | 0.05–0.18 |
| SWADE | *Donelan et al.* [1997] | 12 | 8.9–12.1 | 0.32–0.51 | 5.4–8.7 | 0.05–0.07 |
| HEXOS | *Janssen* [1997] | 28 | 9.1–17.1 | 0.33–0.84 | 9.0–10.6 | 0.04–0.08 |
| All | | 277 | 4.0–18.9 | 0.16–0.84 | 1.8–10.9 | 0.03–0.21 |

is shown in Figure 6. These data are characterized by a near bi-modal distribution of phase velocity. Runs with $c_p \approx 3$ m $s^{-1}$ are short fetch (1–2 km) cases, while the faster waves result from fetches of up to 300 km. The wide range of $c_p$ results in a considerable range of wave age, with some $u_*/c_p$ values double those of the FETCH data set.

[32] The *Anctil and Donelan* [1996] data mentioned earlier are part of the WAVES data base. However while Anctil and Donelan selected their data to study the effects of shoaling on wind stress, the wind sea data considered here exclude such conditions.

### 4.2. AGILE

[33] During the autumn seasons of 1994 and 1995, the 15 m research vessel *AGILE* was used to carry out eddy correlation measurements of momentum, sensible heat, water vapor and carbon dioxide fluxes in the western basin of Lake Ontario. Wave slopes and spectra, and profiles of currents and turbulent kinetic energy dissipation rates were also measured. The stress measurements were made using a Solent 3-axis sonic anemometer mounted on a bow mast at 7.8 m. Full ship motion was measured using gyroscopes, linear accelerometers and a compass, and a motion correction algorithm was applied to the anemometer data, as described above. Details of the experimental set-up, and some preliminary results, are presented by *Donelan and Drennan* [1995]. The sampling strategy during these experiments was to collect data nearly continuously while heading into the wind, with the fetch varying from near zero to 20 km.

[34] Applying the same criteria as discussed above, only pure wind sea data are selected. From the two field seasons, sixty-four runs of 20–25 minutes length met these criteria. The $u_* - c_p$ parameter range of the AGILE data is shown in Figure 6. The data set covers a friction velocity range similar to the FETCH and WAVES data sets, but with peak phase speeds spanning the gap between the other two sets.

### 4.3. SWADE

[35] The Surface Wave Dynamics Experiment, SWADE, took place off the coast of Virginia in 1990–1991. Here we use stress data collected from a K-Gill anemometer mounted on the bow tower of a small ship [*Donelan et al.*, 1997]. The data are corrected for the motion of the ship, and classified according to sea state using directional spectra obtained from a bow mounted wave gauge array. Twelve runs are classified as pure wind sea data using the above criteria. The parameter range of the data is shown in Figure 6.

### 4.4. HEXOS

[36] HEXOS, the Humidity Exchange over the Sea experiment, was conducted in 1986 from a tower at 18 m depth, in the North Sea [*Smith et al.*, 1992]. Early results from HEXOS [*Maat et al.*, 1991] provided support for a strong wave age dependence of the drag coefficient. These data were subsequently found to be influenced by flow distortion around the probe supports, but a re-analysis by *Smith et al.* [1992] showed a similar wave age dependence. *Janssen* [1997] questioned the statistical significance of the HEXOS wave age dependence, while *Oost* [1998] found that some of the higher wind/wave HEXOS data were affected by shoaling.

[37] Here we use the HEXOS data published by *Janssen* [1997], applying the wave criteria of *Oost* [1998] to exclude shoaling conditions. The Janssen data were previously selected to be pure wind sea. We average the stress and mean wind values from the two anemometers, and use only those data from the rough flow regime. Twenty-eight data points meet the criteria. The parameter range of the full wind sea data set (50 points) is shown in Figure 6. The points measured in conditions with peak wavelengths of greater than 80m have been circled: these are the points *Oost* [1998] identified as affected by shoaling. In contrast, *Komen et al.* [1998] presented model results indicating that shoaling is not a problem for these data. In the analysis which follows these data are excluded. However it was found that including these data changes the regression coefficients only by order 0.3%.

## 5. Wave Age Analysis

[38] The combined $u_* - c_p$ parameter space for all five data sets is shown in Figure 6. It covers a range of roughly a factor of five in each of phase speed and friction velocity, and an order of magnitude in wave age. In Figure 7 the dimensionless roughness of the data is plotted versus inverse wave age. The five data sets are seen to exhibit a consistent behavior, with a wave age dependence somewhat steeper than that of *Donelan* [1990], a relationship obtained using earlier Lake Ontario data. For convenience, the relation of *Donelan* [1990], and other wave age relations referenced in the text, are included in Table 2. Henceforth the data are treated as a single data set. We divide the inverse wave age range equally into eight groups, and logarithmically average the data within each group. Here we exclude from the data set three points which lie 5, 3 and 3 standard deviations respectively (about 2 orders of magnitude) above their group means. The results, showing one standard deviation in the logarithms of inverse wave age and dimensionless roughness are plotted in Figure 7.

[39] There is some evidence that the two lowest data groups, corresponding to fully developed conditions, exhibit a different behavior, i.e., a reduced wave age dependence compared with the younger classes. This is consistent with the early work of *Volkov* [1970] who considered fully developed waves, with $0.033 < u_*/c_p < 0.05$, as distinct from developing ones, $u_*/c_p \geq 0.05$. Similarly, *Oost* [1998] noted the existence of several wave age ranges, within each of which the roughness exhibited a different wave age dependence. In particular, for growing waves ($u_*/c_p > 1/17$) the Charnock parameter was found to exhibit a significant wave age dependence, while for waves near full development $\alpha$ was found to be constant.

[40] Following *Volkov* [1970], we consider only the data representing developing seas, $u_*/c_p \geq 0.05$ and find the roughness/wave age relationship as

$$z_o/\sigma = 13.2\left(u_*/c_p\right)^{3.36\pm0.22}, \tag{8}$$

showing 95% confidence limits on the exponent. Equivalent confidence limits on the multiplicative factor yield the range [7.7, 22.6]. If the fully developed waves are retained, the regression yields $z_o/\sigma = 5.0\ (u_*/c_p)^{2.94\pm0.19}$, again showing 95% confidence limits on the exponent. Confidence limits on the multiplier are [3.0, 8.3]. This is closer to the curve of *Donelan* [1990]: the wave age effect is reduced, but remains

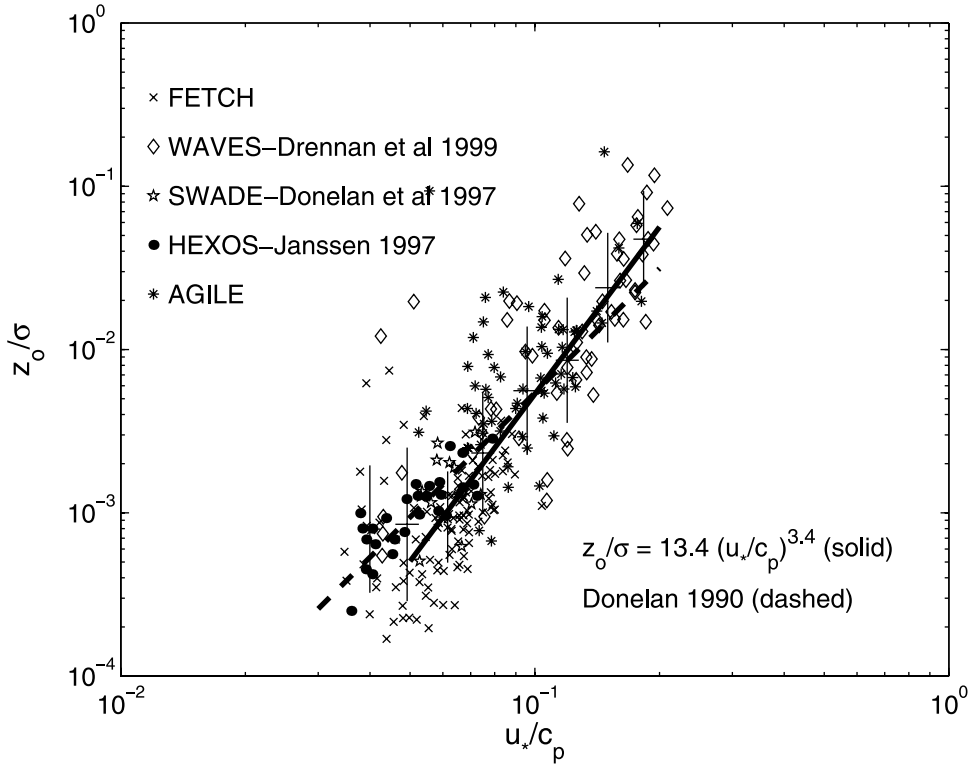


**Figure 7.** Dimensionless roughness versus inverse wave age for pure wind data meeting the rough flow criterion $z_o u_*/\nu > 2.3$. Here $z_o$ is the roughness length, $\sigma$ is the standard deviation of the surface elevation, $u_*$ is the friction velocity, $c_p$ is the peak wave phase speed, and $\nu$ is the kinematic viscosity of air. Data sources are identified on the plot. The data are grouped into eight classes of equal size, with the crosses indicating 1 standard deviation in $\log(z_o/\sigma)$ and $\log(u_*/c_p)$ for each class. The curves are from *Donelan* [1990] (dashed) and the relationship proposed here (solid).

significant. This is in contrast to the HEXOS results, where the inclusion of the fully developed data removed the significance of the wave age dependence [*Oost*, 1998].

[41] As discussed above, even with the large parameter range there is still the possibility that the regression is affected by spurious correlation in that both the dimensionless roughness and wave age are dependent on the friction velocity. In order to investigate this, we separate the data into six groups based on the friction velocity: $u_* \leq 0.3$, $0.3 < u_* \leq 0.4$, …, $u_* > 0.7$ m s$^{-1}$. By grouping the data this way, almost all of the variability in wave age is due to variability in phase speed. The data (excluding the fully developed cases, $u_*/c_p < 0.05$) are replotted in Figure 8, with each range denoted by a different symbol. For each of the groups, a linear regression between $\log(z_o/\sigma)$ and $\log(u_*/c_p)$ was carried out. The six regression lines are plotted in Figure 8, and the coefficients are given in Table 3.

[42] The best fit (logarithmic) for the lowest $u_*$ group is significantly different from the others at the 95% confidence level. That is, null hypothesis tests based on these data reject the best fits derived from the other groups at the 95% confidence level. Similarly, null hypotheses based on the other groups reject the fit of this group at the same level. This group has a larger percentage variability in $u_*$, and a smaller range of $c_p$ than the others (Figure 6), and so may be affected by spurious correlation. Within the considerable scatter of the data, the remaining lines are equivalent (again, using null hypothesis tests at the 95% confidence level). Hence, we use a single curve, the average of the remaining five regression lines, to describe the wave age relationship of the data set:

$$z_o/\sigma = 13.4\left(u_*/c_p\right)^{3.4}. \tag{9}$$

This curve, plotted in Figures 7 and 8, is taken to be the best regression for the data set. It is not significantly different from (8), indicating that spurious correlation may not be a significant problem with our original correlation.

[43] It is interesting that the inclusion of the fully developed data in the $u_*$ groups does not significantly alter the regressions (see Table 3). See especially the $0.3 < u_* \leq 0.4$ group, where the inclusion has nearly doubled the size of the group, but with negligible effect on the regression. Again, omitting the lowest $u_*$ group due to possible spurious correlation, the mean of the regressions of the remain-

**Table 2.** Referenced Wave Age Relations

| Reference | Relationship |
|---|---|
| *Charnock* [1955] | $z_o g/u_*^2 = \alpha$ |
| *Maat et al.* [1991] | $z_o g/u_*^2 = 0.8\ (u_*/c_p)^{1.0}$ |
| *Smith et al.* [1992] | $z_o g/u_*^2 = 0.48\ (u_*/c_p)^{1.0}$ |
| *Johnson et al.* [1998] | $z_o g/u_*^2 = 1.89\ (u_*/c_p)^{1.59}$ |
| This study | $z_o g/u_*^2 = 1.7\ (u_*/c_p)^{1.7}$ |
| *Donelan* [1990] | $z_o/\sigma = 1.84\ (u_*/c_p)^{2.53}$ |
| This study | $z_o/\sigma = 13.4\ (u_*/c_p)^{3.4}$ |

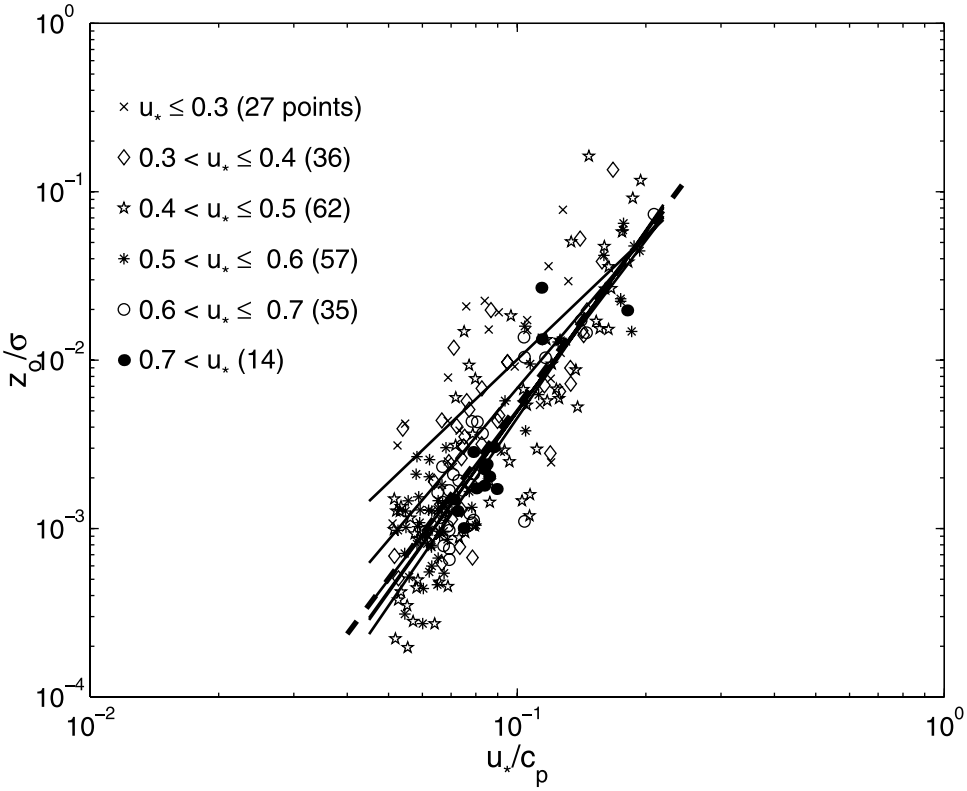


**Figure 8.** Dimensionless roughness versus inverse wave age for developing wind sea ($u_*/c_p \geq 0.05$), rough flow data. The data are grouped according to $u_*$ and a regression made for each group. The regression coefficients are given in Table 3. The mean regression line for data from the five higher $u_*$ classes is also shown (dashed).

ing 5 classes yields $z_o/\sigma = 11.2(u_*/c_p)^{3.3}$, which is close to (9). Consequently, the wave age relationship (9) may well apply for both fully developed and developing sea.

## 6. Charnock Parameterization

[44] It has been common to use the Charnock parameter, $\alpha = z_o g/u_*^2$ for the dimensionless roughness. As this parameterization does not explicitly include any information on the wave field, it is conveniently used in atmospheric models. In Figure 9 we plot our data set as $\alpha$ versus inverse wave age, again restricting the data to developing waves. Although there is considerably more scatter using this representation of roughness, regressions of the data grouped by $u_*$ again yield consistent slopes. Again ignoring the lowest $u_*$ bin, the mean of the regression lines yields

$$z_o g/u_*^2 = 1.7\left(u_*/c_p\right)^{1.7}. \tag{10}$$

This is close to the relation of *Johnson et al.* [1998], based on several experiments, but shows a stronger wave age dependence than the HEXOS relation of *Smith et al.* [1992]. Both relations are given in Table 2 and shown on Figure 9. Once again, the inclusion of the fully developed data in the regression does not significantly change the fit (see Table 4).

[45] Equations (9) and (10) give us two different expressions for the roughness as a function of wave age. To verify their consistency, it is necessary to relate the wave height parameter $\sigma$ of (9) to the wind and wave age. We use an empirical relationship between $\sigma$ and an alternative form of inverse wave age, $U_{10N}/c_p$, derived from field data in Lake Ontario [*Donelan et al.*, 1993]:

$$\sigma = 0.055\left(U_{10N}^2/g\right)\left(U_{10N}/c_p\right)^{-1.7}. \tag{11}$$

Using (11), and the definition of $C_{10N}$, in (9) we have

$$z_o = (13.4)(0.055)\left(U_{10N}^2/g\right)C_{10N}^{0.85}\left(u_*/c_p\right)^{1.7}. \tag{12}$$

**Table 3.** Regression Constants log($a$) and $b$ in Relation $z_o/\sigma = a(u_*/c_p)^b$ for Different $u_*$ Ranges[a]

| | | $u_*/c_p \geq 0.05$ | | All Wind Sea Data | |
|---|---|---|---|---|---|
| $u_*$ Range | N | log($a$) | $b$ | log($a$) | $b$ |
| $u_* \leq 0.3$ | 27 (36) | 1.0 ± 2.4 | 2.4 ± 1.0 | 0.3 ± 1.6 | 2.1 ± 0.6 |
| $0.3 < u_* \leq 0.4$ | 36 (56) | 1.9 ± 1.7 | 3.0 ± 0.7 | 1.5 ± 0.9 | 2.8 ± 0.3 |
| $0.4 < u_* \leq 0.5$ | 62 (75) | 2.9 ± 1.1 | 3.6 ± 0.5 | 2.4 ± 0.9 | 3.3 ± 0.4 |
| $0.5 < u_* \leq 0.6$ | 57 (58) | 2.4 ± 0.5 | 3.3 ± 0.2 | 2.3 ± 0.6 | 3.3 ± 0.2 |
| $0.6 < u_* \leq 0.7$ | 35 (35) | 2.8 ± 0.8 | 3.5 ± 0.3 | 2.8 ± 0.8 | 3.5 ± 0.3 |
| $0.7 < u_*$ | 14 (14) | 3.1 ± 1.7 | 3.7 ± 0.7 | 3.1 ± 1.7 | 3.7 ± 0.7 |
| Average ($u_* > 0.3$) | 231 (274) | 2.6 | 3.4 | 2.4 | 3.3 |

[a]Values are given for developing seas $u_*/c_p \geq 0.05$ and the full pure wind sea data set. The 95% confidence ranges are indicated. N is the number of points in each class, with the number in the full data set in braces.

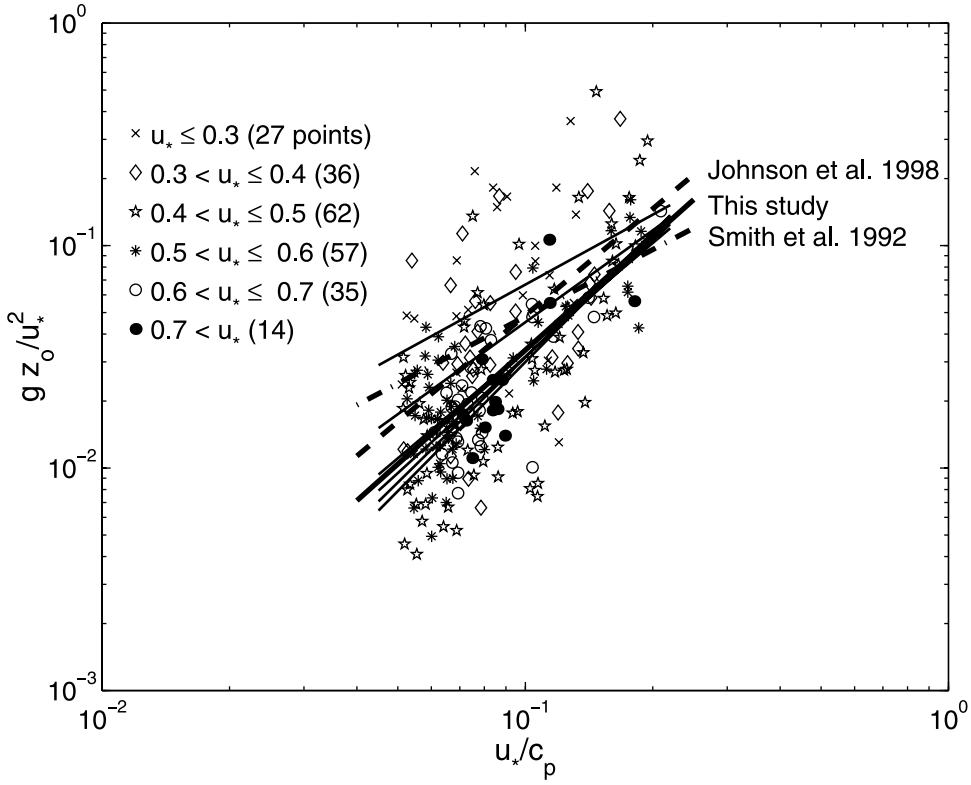


**Figure 9.** Charnock parameter versus inverse wave age for developing wind sea ($u_*/c_p \geq 0.05$) rough flow data. The data are grouped according to $u_*$ and a regression made for each group. The regression coefficients are given in Table 4. The curves are from *Smith et al.* [1992] (dash-dotted), *Johnson et al.* [1998] (dashed), and the mean regression line for data from the five higher $u_*$ classes (solid).

Equations (10) and (12) have the same wave age dependence. Comparing the multiplicative factors, using $z_{ch}$ to denote the roughness derived in (10), we have after some simplification

$$z_o/z_{ch} = 0.43 C_{10N}^{-0.15}. \tag{13}$$

Using typical values of $C_{10N}$ (0.001 to 0.0015), we have $z_o/z_{ch}$ between 1.14 and 1.21. Hence, the two dimensionless representations of roughness, (9) and (10), yield a very similar wave age dependence, with drag coefficients from the former roughly 3% larger than those from (10).

[46] Using (6) and (10), we can determine parametric curves for the drag coefficient in terms of wind speed and wave age. Several curves spanning the range of FETCH values are plotted in Figure 10. The FETCH wind sea data appear on the plot grouped by wave age, and averaged in 3 m s$^{-1}$ wind speed bins. The strongly forced developing sea data (stars and circles) show a clear wave age dependence, with values well above those predicted by *Smith* [1980], though slightly less (on average) than predicted by (6) and (10). This is consistent with Figure 7, where the FETCH data are seen to be less rough, on average, than is predicted by (9). The Smith relationship is seen to be representative of near fully developed wind sea conditions, with $u_*/c_p \approx 0.04-0.05$. The drag coefficients associated with the lowest wind speed group, $\overline{U_{10N}} = 7.3$ m s$^{-1}$ with waves near full development ($\overline{u_*/c_p} = 0.047$), are considerably higher than predicted. The significance of this is unclear, as the group size is small, and the scatter within the group large.

[47] There clearly remains significant scatter in the data, which is not explained by the wave age dependent relations. Much of this is likely attributable to sampling variability. Other sources of variability include nonstationarity, boundary layer depth [e.g., *Mahrt et al.*, 1998], and large scale atmospheric features such as internal waves or roll cells [e.g., *Chen et al.*, 2001]. According to *Donelan* [1990], the estimated sampling error in individual 28.5 min FETCH estimates of $-\overline{u'w'} \approx u_*^2$ ranges from 9% (at $U_7 = 15$ m s$^{-1}$) to 16% (at $U_7 = 5$ m s$^{-1}$). *Komen et al.* [1998] estimate the error in $u_*$ as roughly 10%. Assuming errors (sampling and otherwise) of several per cent in $U$, $Z$, $L$, etc., a conservative estimate of the error of individual $C_{10N}$ values is 20%. Consequently, it is not surprising that while the wave age

**Table 4.** Regression Constants log($a$) and $b$ in Relation $z_o g/u_*^2 = a(u_*/c_p)^b$ for Different $u_*$ Ranges[a]

| | | $u_*/c_p \geq 0.05$ | | All Wind Sea Data | |
|---|---|---|---|---|---|
| $u_*$ Range | N | log($a$) | $b$ | log($a$) | $b$ |
| $u_* \le 0.3$ | 27 (36) | $-0.3 \pm 2.4$ | $1.0 \pm 1.0$ | $-1.3 \pm 1.6$ | $0.6 \pm 0.6$ |
| $0.3 < u_* \le 0.4$ | 36 (56) | $0.1 \pm 1.5$ | $1.4 \pm 0.6$ | $-0.4 \pm 0.8$ | $1.2 \pm 0.3$ |
| $0.4 < u_* \le 0.5$ | 62 (75) | $0.8 \pm 1.0$ | $1.9 \pm 0.4$ | $0.3 \pm 0.9$ | $1.6 \pm 0.3$ |
| $0.5 < u_* \le 0.6$ | 57 (58) | $0.3 \pm 0.4$ | $1.6 \pm 0.2$ | $0.2 \pm 0.5$ | $1.5 \pm 0.2$ |
| $0.6 < u_* \le 0.7$ | 35 (35) | $0.5 \pm 0.6$ | $1.7 \pm 0.2$ | $0.5 \pm 0.6$ | $1.7 \pm 0.2$ |
| $0.7 < u_*$ | 14 (14) | $0.9 \pm 1.1$ | $1.9 \pm 0.5$ | $0.9 \pm 1.1$ | $1.9 \pm 0.5$ |
| Average ($u_* > 0.3$) | 231 (274) | 0.5 | 1.7 | 0.3 | 1.6 |

[a]Values are given for developing seas $u_*/c_p \geq 0.05$ and the full pure wind sea data set. The 95% confidence ranges are indicated. N is the number of points in each class, with number in the full data set in braces.

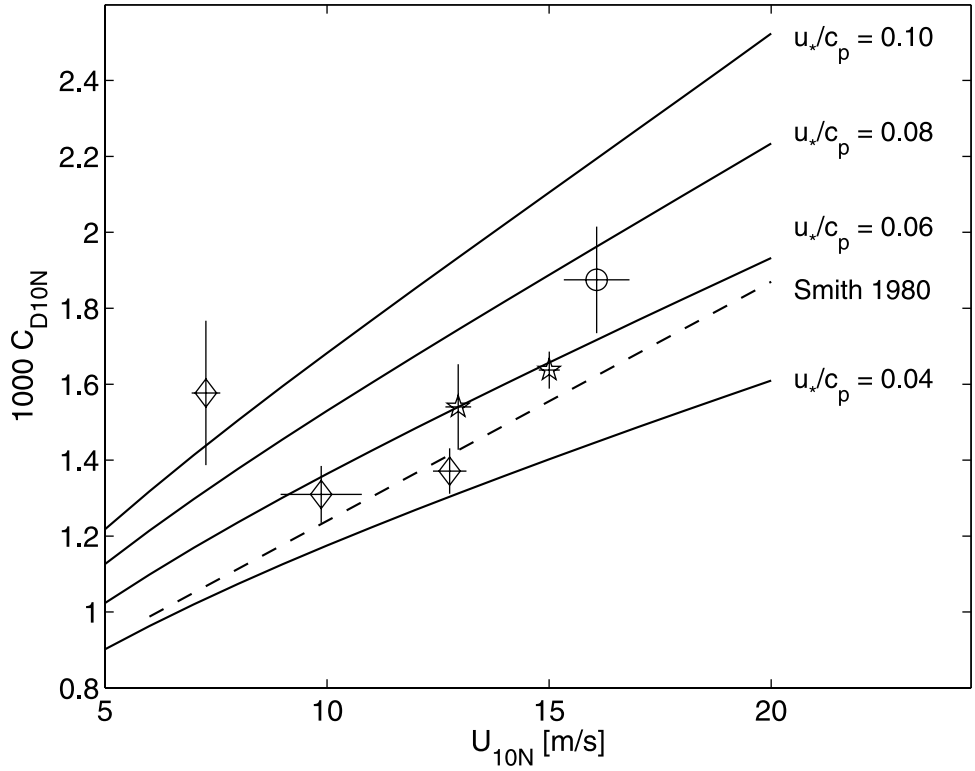


**Figure 10.** Drag coefficient versus wind speed, both 10 m neutral, for FETCH wind sea data. The data are grouped by inverse wave age, $0.04 < u_*/c_p \leq 0.06$ (diamonds), $0.06 < u_*/c_p \leq 0.08$ (stars), $u_*/c_p > 0.08$ (circles), in wind speed bins of 3 m $s^{-1}$, with the crosses indicating 2 standard errors in $C_{D10N}$ and $U_{10N}$. The curves are from *Smith* [1980] and the wave age dependent drag relations resulting from equations (6) and (10).

dependent drag relations are in good general support of the data, individual points are not as well predicted.

## 7. Conclusions

[48] Using five field data sets, we have investigated the wave age dependence of the surface wind stress. The data were selected as representative of pure wind seas, deep water, and fully rough flow. In these conditions, Monin-Obukhov theory is expected to hold, and a unique relationship between drag coefficient (or surface roughness) and wave age is expected. For developing waves, it was found that $z_o/\sigma = 13.4\ (u_*/c_p)^{3.4}$, which implies a significant wave age effect in the drag coefficient. The inclusion of fully developed wind sea data in the regression did not significantly change the result. This relationship was found using a procedure that minimizes the likelihood of spurious correlation in friction velocity. Finally, the wave age relationship was shown to be consistent with that derived using the Charnock form of the dimensionless roughness, $z_o g/u_*^2 = 1.7\ (u_*/c_p)^{1.7}$. It is clear that drag coefficients during fetch- or duration- limited high wind events, such as Mistrals, are not well predicted by traditional bulk relations. The wave age based relations presented here offer significant improvement.

[49] These results provide strong support for a wave age dependence of roughness as proposed by *Kitaigorodskii and Volkov* [1965]. These are not the first data to provide this support, but they are the first with a wide enough parameter range to effectively eliminate the effects of spurious self-correlation in $u_*$ which have plagued many other studies. The utility of these results is particularly high for the communities developing coupled air-sea models. Wave age dependence has been recognized as a significant factor, and this work provides some of the parameterizations necessary for further progress in these fields.

[50] The present results were obtained for pure wind sea conditions, and this is a clear limitation to their general applicability. Pure or dominant wind seas are frequent in coastal regions, and bounded seas, and during high wind events, but swells are generally present in the open ocean. Although it seems likely that the results will hold in mixed seas with light-moderate swell, this remains to be tested. The challenge for the future is to develop a single parameterization, one valid not just in pure wind seas, but also swell dominated, mixed sea and depth-limited conditions. Given that Monin-Obukhov similarity theory (which forms the basis for the parameterization) can not be assumed valid in all these conditions, it seems that the first steps to achieving this goal must include the development of a modified MO theory.

[51] **Acknowledgments.** We thank the following people who contributed to the success of this work: M. Donelan and M. Rebozo (RSMAS), L. Eymard (CETP), H. Dupuis (DGO-Bordeaux), J. Gabriele and J. Cooper (NWRI, Canada), as well as the officers and crew of the N.O. *L'Atalante*, and the FETCH team. In addition, we gratefully acknowledge support for the FETCH experiment from the European Community MAST programme, grant CEE MAS3.CT96.0051, and from the French "Institut National des Sciences de l'Univers" (PATOM and PNTS grants). WD also acknowl-

edges partial support from ONR (N00014-94-1-0629) and NSF (OCE-9871855) for the AGILE experiment, and from the Royal Caribbean Junior Faculty Fund for travel.

## References


Anctil, F., and M. A. Donelan, Air-water momentum flux observations over shoaling waves, *J. Phys. Oceanogr.*, *26*, 1344–1353, 1996.

Anctil, F., M. A. Donelan, W. M. Drennan, and H. C. Graber, Eddy correlation measurements of air-sea fluxes from a Discus buoy, *J. Atmos. Oceanic Technol.*, *11*, 1144–1150, 1994.

Capon, J., High-resolution frequency-wavenumber spectrum analysis, *Proc. IEEE*, *57*, 1408–1418, 1969.

Charnock, H., Wind stress on a water surface, *Q. J. R. Meteorol. Soc.*, *81*, 639–640, 1955.

Chen, W., M. L. Banner, E. J. Walsh, J. B. Jensen, and S. Lee, The Southern Ocean Waves Experiment, part II, Sea surface response to wind speed and wind stress variations, *J. Phys. Oceanogr.*, *31*, 174–198, 2001.

DeCosmo, J., K. B. Katsaros, S. D. Smith, R. J. Anderson, W. A. Oost, K. Bumke, and H. Chadwick, Air-sea exchange of water and sensible heat: The Humidity Exchange Over the Sea (HEXOS) results, *J. Geophys. Res.*, *101*, 12,001–12,016, 1996.

Donelan, M. A., The dependence of the aerodynamic drag coefficient on wave parameters, paper presented at 1st International Conference on Meteorology and Air-Sea Interaction of the Coastal Zone, Am. Meteorol. Soc., Boston, Mass., 1982.

Donelan, M. A., Air-sea interaction, in *The Sea*, vol. 9, *Ocean Engineering Science*, edited by B. LeMéhauté and D. Hanes, pp. 239–292, John Wiley, New York, 1990.

Donelan, M. A., and W. M. Drennan, Direct field measurements of the flux of carbon dioxide, in *Air-Water Gas Transfer*, edited by B. Jähne and E. C. Monahan, pp. 677–683, Aeon-Verlag, Hanau, Germany, 1995.

Donelan, M. A., J. Hamilton, and W. H. Hui, Directional spectra of wind generated waves, *Philos. Trans. R. Soc. London, Ser. A*, *315*, 509–562, 1985.

Donelan, M. A., F. W. Dobson, S. D. Smith, and R. J. Anderson, On the dependence of sea surface roughness on wave development, *J. Phys. Oceanogr.*, *23*, 2143–2149, 1993.

Donelan, M. A., W. M. Drennan, and K. B. Katsaros, The air-sea momentum flux in mixed wind sea and swell conditions, *J. Phys. Oceanogr.*, *27*, 2087–2099, 1997.

Donelan, M. A., N. Madsen, K. K. Kahma, I. K. Tsanis, and W. M. Drennan, Apparatus for atmospheric boundary layer measurements over waves, *J. Atmos. Oceanic Technol.*, *16*, 1172–1182, 1999.

Drennan, W. M., M. A. Donelan, N. Madsen, K. B. Katsaros, E. A. Terray, and C. N. Flagg, Directional wave spectra from a Swath ship at sea, *J. Atmos. Oceanic Technol.*, *11*, 1109–1116, 1994.

Drennan, W. M., H. C. Graber, M. A. Donelan, and E. A. Terray, Directional wave measurements from the ASIS (air-sea interaction spar) buoy, paper presented at Oceans98, IEEE Oceanic Eng. Soc., Nice, France, 1998.

Drennan, W. M., K. K. Kahma, and M. A. Donelan, On momentum flux and velocity spectra over waves, *Boundary Layer Meteorol.*, *92*, 489–515, 1999.

Dupuis, H., C. Guerin, D. Hauser, A. Weill, P. Nacass, W. M. Drennan, S. Cloché, and H. C. Graber, Impact of flow distortion corrections on turbulent fluxes estimated by the inertial dissipation method during the FETCH experiment on R/V *Atalante*, *J. Geophys. Res.*, *108*, doi:10.1029/2001JC01075, in press, 2003.

Edson, J. B., and C. W. Fairall, Similarity relationships in the marine atmospheric surface layer for terms in the TKE and scalar variance budgets, *J. Atmos. Sci.*, *55*, 2311–2328, 1998.

Geernaert, G. L., Bulk parameterization for the wind stress and heat fluxes, in *Surface Waves and Fluxes*, edited by G. L. Geernaert and W. J. Plant, pp. 91–172, Kluwer Acad., Norwell, Mass., 1990.

Geernaert, G. L., K. B. Katsaros, and K. Richter, Variations of the drag coefficient and its dependence on sea state, *J. Geophys. Res.*, *91*, 7667–7679, 1986.

Gerling, T. W., Partitioning sequences and arrays of directional ocean wave spectra into component wave systems, *J. Atmos. Oceanic Technol.*, *9*, 444–458, 1992.

Graber, H. C., E. A. Terray, M. A. Donelan, W. M. Drennan, J. Van Leer, and D. B. Peters, ASIS—A new air-sea interaction spar buoy: Design and performance at sea, *J. Atmos. Oceanic Technol.*, *17*, 708–720, 2000.

Hauser, D., et al., The FETCH experiment: An overview, *J. Geophys. Res.*, *108*(C3), 8053, doi:10.1029/2001JC001202, 2003.

Hodur, R. M., The Naval Research Laboratory's Coupled Ocean/Atmosphere Mesoscale Prediction System (COAMPS), *Mon. Weather Rev.*, *125*, 1414–1430, 1997.

Janssen, J. A. M., Does wind stress depend on sea state or not? A statistical analysis of HEXMAX data, *Boundary Layer Meteorol.*, *83*, 479–503, 1997.

Janssen, P. A. E. M., Wave-induced stress and the drag of air flow over sea waves, *J. Phys. Oceanogr.*, *19*, 745–754, 1989.

Johnson, H. K., J. Højstrup, H. J. Vested, and S. E. Larsen, On the dependence of sea surface roughness on wind waves, *J. Phys. Oceanogr.*, *28*, 1702–1716, 1998.

Kenney, B. C., Beware of spurious self-correlations!, *Water Resources Res.*, *18*, 1041–1048, 1982.

Kitaigorodskii, S. A., *The Physics of Air-Sea Interaction* (in Russian), Gidrometeorologicheskoe Izdatel'stvo, Leningrad, 1970. (Isr. Program for Sci. Transl., Jerusalem, 1973)

Kitaigorodskii, S. A., and Y. A. Volkov, On the roughness parameter of the sea surface and the calculation of momentum flux in the near-water layer of the atmosphere, *Izv. Acad. Sci. USSR Atmos. Oceanic Phys., Engl. Transl.*, *1*, 973–988, 1965.

Komen, G., L. Cavaleri, M. Donelan, K. Hasselman, S. Hasselman, and P. A. E. M. Janssen, *Dynamics and Modelling of Ocean Waves*, Cambridge Univ. Press, 532 pp., 1994.

Komen, G., P. A. E. M. Janssen, V. Makin, and W. Oost, On the sea state dependence of the Charnock parameter, *Global Atmos. Ocean. Syst.*, *5*, 367–388, 1998.

Maat, N., C. Kraan, and W. A. Oost, The roughness of wind waves, *Boundary Layer Meteorol.*, *54*, 89–103, 1991.

Mahrt, L., D. Vickers, J. Howell, J. Højstrup, J. M. Wilczak, J. Edson, and J. Hare, Sea surface drag coefficients in the Risø Air Sea Experiment, *J. Geophys. Res.*, *101*, 14,327–14,335, 1996.

Mahrt, L., D. Vickers, J. Edson, J. Sun, J. Højstrup, J. Hare, and J. M. Wilczak, Heat flux in the coastal zone, *Boundary Layer Meteorol.*, *86*, 421–446, 1998.

Makin, V. K., and C. Mastenbroek, Impact of waves on air-sea exchange of sensible heat and momentum, *Boundary Layer Meteorol.*, *79*, 279–300, 1996.

Miyake, M., R. W. Stewart, and R. W. Burling, Spectra and cospectra of turbulence over water, *Q. J. R. Meteorol. Soc.*, *96*, 138–143, 1970.

Monin, A. S., and A. M. Obukhov, Basic laws of turbulent mixing in the ground layer of the atmosphere, *Akad. Nauk. SSSR Geofiz. Inst. Tr.*, *151*, 163–187, 1954.

Noh, Y., Dynamics of diurnal thermocline formation in the oceanic mixed layer, *J. Phys. Oceanogr.*, *26*, 2183–2195, 1996.

Oost, W. A., The KNMI HEXMAX stress data: A reanalysis, *Boundary Layer Meteorol.*, *86*, 447–468, 1998.

Pettersson, H., H. C. Graber, D. Hauser, C. Quentin, K. K. Kahma, W. M. Drennan, and M. A. Donelan, Directional wave measurements from three wave sensors during the FETCH experiment, *J. Geophys. Res.*, *108*, doi:10.1029/2001JC01164, in press, 2003.

Phillips, O. M., *The Dynamics of the Upper Ocean*, 2nd ed., 336 pp., Cambridge Univ. Press, New York, 1977.

Powers, J. G., and M. T. Stoelinga, A coupled air-sea mesoscale model: Experiments in atmospheric sensitivity to marine roughness, *Mon. Weather Rev.*, *128*, 208–228, 2000.

Rieder, K. F., Analysis of sea-surface drag parameterizations in open ocean conditions, *Boundary Layer Meteorol.*, *82*, 355–377, 1997.

Smedman, A. S., U. Högström, H. Bergström, A. Rutgersson, K. K. Kahma, and H. Pettersson, A case study of air-sea interaction during swell conditions, *J. Geophys. Res.*, *104*, 25,833–25,852, 1999.

Smith, S. D., Wind stress and heat flux over the ocean in gale force winds, *J. Phys. Oceanogr.*, *10*, 709–726, 1980.

Smith, S. D., Water vapor flux at the sea surface, *Boundary Layer Meteorol.*, *47*, 277–293, 1989.

Smith, S. D., et al., Sea surface wind stress and drag coefficients: The HEXOS results, *Boundary Layer Meteorol.*, *60*, 109–142, 1992.

Stewart, R. W., The wave drag of wind over water, *J. Fluid Mech.*, *10*, 189–194, 1961.

Volkov, Y. A., Turbulent flux of momentum and heat in the atmospheric surface layer over a disturbed surface, *Izv. Acad. Sci. USSR Atmos. Oceanic Phys., Engl. Transl.*, *6*, 770–774, 1970.


W. M. Drennan and H. C. Graber, Rosenstiel School of Marine and Atmospheric Science, University of Miami, 4600 Rickenbacker Causeway, Miami, FL 33149, USA. (wdrennan@rsmas.miami.edu; hgraber@rsmas.miami.edu)

D. Hauser and C. Quentin, Centre d'étude des Environnements Terrestres et Planétaires (CETP), 10–12 Avenue de l'Europe, F-78140 Vélizy, France. (hauser@cetp.ipsl.fr; celine.quentin@cetp.ipsl.fr)